

Horizon 2020 Program (2014-2020)  
**FET-Open Novel ideas for radically new technologies**  
**FETOPEN-01-2018-2019-2020**



Architecting More than Moore – Wireless Plasticity for  
Massive Heterogeneous Computer Architectures <sup>†</sup>

**D1.2: Graphene Integration Design Report**

Contractual Date of Delivery	31/12/2021
Actual Date of Delivery	06/01/2022
Deliverable Security Class	Public
Editor	Elana Santana (UoS)
Contributors	Elana Santana (UoS) Peter Haring Bolívar (UoS) Mohamed Elsayed (RWTH) Zhenxing Wang (AMO)
Quality Assurance	Max Lemme (AMO) Eduard Alarcón (UPC)

---

<sup>†</sup> This project is supported by the European Commission under the Horizon 2020 Program with Grant agreement no: 863337

## Document Revisions & Quality Assurance

Deliverable Number	D1.2
Deliverable Responsible	UoS
Work Package	WP1
Main Editor	Elana Santana (UoS)

### Internal Reviewers

1. Max Lemme (AMO)
2. Eduard Alarcón (UPC)

### Revisions

Version	Date	By	Overview
1.2.5	06/01/2022	P. Haring Bolívar (UoS)	Final version after input from RWTH
1.2.4	28/12/2021	P. Haring Bolívar (UoS)	Final version after internal review
1.2.3	03/12/2021	Elana Santana (UoS)	First complete version.
1.2.2	03/12/2021	Zhenxing Wang (AMO)	Adding AMO contribution.
1.2.1	01/12/2021	Mohamed Elsayed (RWTH)	Adding RWTH contribution.
1.2.0	23/11/2021	Elana Santana (UoS)	First draft with UoS contribution.

### Legal Disclaimer

The information in this document is provided “as is”, and no guarantee or warranty is given that the information is fit for any particular purpose. The above referenced consortium members shall have no liability to third parties for damages of any kind including without limitation direct, special, indirect, or consequential damages that may result from the use of these materials subject to any liability which is mandatory due to applicable law. © 2019 by WiPLASH Consortium.

## Executive Summary

This deliverable is the second report from WP1 RF Design and Implementation, which aims to present designs for graphene component integration with WP2 Technological Integration and a quantitative analysis of the performance advantages with respect to conventional technologies. In order to integrate the graphene antenna with the transmitter circuit, a compatible integration process needs to be established.

A graphene antenna that is driven electrically was developed in order to be integrated to the future transmitter chips. The antenna is a graphene patch driven electrically by its ground-signal-ground (GSG) pads. The substrate material - Polyimide - was chosen due to an already well established manufacturing process at AMO. Graphene-based devices on polyimide substrates were already produced by AMO in the past showing good graphene mobility.

In this deliverable, the structure and simulation results of a graphene patch antenna for future integration are described. The simulation results are presented and discussed. The University of Siegen (UoS) performed a series of simulation analysis and was able to compare the performance of a graphene patch antenna to a standard metal patch antenna. The resonant frequency shown by the graphene patch antenna was smaller compared to its metal counterpart. Besides, by changing the graphene Fermi level, the resonant frequency of the antenna could be tuned. It is worth to note that, according to simulations, a high graphene mobility is needed so that a graphene patch has an acceptable antenna behavior.

Regarding the development in the graphene-based devices and circuits, we improved our in-house graphene-based MMIC to preserve the quality of the used graphene. Accordingly, we exploited our graphene diodes in different microwave/mmm-Wave circuit applications.

## Abbreviations and Acronyms

<b>APS</b>	Analogue phase-shifter
<b>CG</b>	Conversion Gain
<b>CPW</b>	Coplanar Waveguide
<b>DR</b>	Dynamic Range
<b>G</b>	Gain
<b>GSG</b>	Ground-signal-ground
<b>MMIC</b>	Monolithic Microwave Integrated Circuit
<b>PD</b>	Power detector
<b>Prad</b>	Radiated Power
<b>NLTL</b>	Nonlinear Transmission Line
<b>RF</b>	Radio-frequency
<b>SiGe</b>	Silicon-Germanium
<b>TFR</b>	Thin film resistor
<b>TRx</b>	Transceiver
<b>U</b>	Power intensity
<b>TM<sub>010</sub></b>	First order dominant mode
<b>f<sub>r010</sub></b>	Resonant frequency
<b>ε<sub>r</sub></b>	Dielectric constant
<b>C<sub>0</sub></b>	Velocity of light
<b>V<sub>f</sub></b>	Fermi velocity
<b>E<sub>f</sub></b>	Fermi energy
<b>τ</b>	Relaxation time

**The *WiPLASH* consortium is composed by:**

UPC	Coordinator	Spain
IBM	Beneficiary	Switzerland
UNIBO	Beneficiary	Italy
EPFL	Beneficiary	Switzerland
AMO	Beneficiary	Germany
UoS	Beneficiary	Germany
RWTH	Beneficiary	Germany



IBM **Research** | Zurich





## Table of Contents

<b>DOCUMENT REVISIONS &amp; QUALITY ASSURANCE</b> .....	<b>2</b>
<b>EXECUTIVE SUMMARY</b> .....	<b>3</b>
<b>ABBREVIATIONS AND ACRONYMS</b> .....	<b>4</b>
<b>TABLE OF CONTENTS</b> .....	<b>7</b>
<b>LIST OF FIGURES</b> .....	<b>8</b>
<b>LIST OF TABLES</b> .....	<b>9</b>
<b>1 INTRODUCTION</b> .....	<b>10</b>
<b>2 GRAPHENE COMPONENTS DESIGNS, SIMULATIONS AND MEASUREMENTS</b> .....	<b>12</b>
2.1 GRAPHENE PATCH ANTENNA DESIGN.....	12
2.2 GRAPHENE PATCH ANTENNA SIMULATION RESULTS.....	13
2.3 GRAPHENE BASED CIRCUITS DESIGN.....	15
2.3.1 <i>Graphene diode-based APS</i> .....	16
2.3.2 <i>Graphene diode-based 60GHz PD with 70dB Dynamic Range</i> .....	17
2.3.3 <i>Graphene diode-based NLTL-based harmonic generator</i> .....	17
2.4 GRAPHENE BASED CIRCUITS MEASUREMENT RESULTS.....	18
2.4.1 <i>Graphene diode-based APS</i> .....	18
2.4.2 <i>Graphene diode-based 60GHz PD with 70dB Dynamic Range</i> .....	19
2.4.3 <i>Graphene diode-based NLTL-based harmonic generator</i> .....	19
<b>3 GRAPHENE COMPONENTS INTEGRATION</b> .....	<b>20</b>
<b>4 SUMMARY OF RESULTS</b> .....	<b>21</b>
<b>BIBLIOGRAPHY</b> .....	<b>22</b>

## List of Figures

Figure 1: Illustration of a patch antenna [1] .....	10
Figure 2: Illustration of the fringing fields of a microstrip.....	10
Figure 3: Representation of a CPW [2] .....	11
Figure 4: Graphene patch antenna simulated in CST. The antenna consists of a metal or graphene patch on top of a dielectric substrate backed by a metal plane. The antenna is driven by the GSG pads. ....	12
Figure 5: S11 simulated values for metal patch (dashed line) and graphene patch with different conductivity values (continuous lines) .....	13
Figure 6: S11 simulation results for graphene patches with different fermi levels and relaxation time 1.2ps (continuous lines) and for a metal patch (dashed lines) .....	14
Figure 7: S11 simulation results for graphene patches with different relaxation times and Fermi level 1.2 eV (continuous lines) and metal patch (dashed line) .....	14
Figure 8: Maximum gain over frequency in dB of graphene patches with different conductivities (continuous lines) and metal patch (dashed line) .....	14
Figure 9: Old MMIC (left) versus the new MMIC (right) .....	15
Figure 10: Raman-shift spectroscopy after fabricating the samples .....	15
Figure 11: Short-circuit current responsivity comparison between different diode families..	16
Figure 12: Graphene-based APS: schematic (left) and chip micrograph (right) .....	17
Figure 13: Graphene-based PD: schematic (left) and chip micrograph (right).....	17
Figure 14: Graphene-based NLTL: schematic (left) and chip micrograph (right).....	18
Figure 15: Measurements of the Graphene-based APS: dB(S <sub>11</sub> ) (left) and phase(S <sub>21</sub> ) (right).	18
Figure 16: Measurements of the Graphene-based PD: input matching (left) and voltage sensitivity (right) .....	19
Figure 17: Measured conversion gain results of the Graphene-based NLTL: second harmonic (left) third harmonic (right) .....	19
Figure 18: Integration strategy with graphene patch antenna on polyimide .....	20

## List of Tables

Table 1: Graphene patch dimensions.....12

# 1 Introduction

The WiPLASH project vision of using graphene-based devices for intra-chip communication in the THz range can bring advantages compared to the ones based on standard technologies, since by recent publications [1], [2], [3], [4], graphene-based antennas, for example, could save chip area and cost, and at the same time, expand capabilities such as to be tunable due to its characteristic electronic energy band dispersion.

To simplify the design of a graphene-based antenna and enhance the future integration, a microstrip antenna approach was adopted due to its ease of fabrication and later on-chip characterization.

A microstrip antenna consists of a metal patch on top of a dielectric substrate with a thickness in the order of  $0.003 \cdot \lambda$  to  $0.05 \cdot \lambda$  of wavelength  $\lambda$  backed by a metal plane [1]. The metal patch can be of any format, but it is commonly designed as a square, rectangular or circular element. Exciting the proper mode under the patch can lead to a maximum radiation pattern that is normal to the patch [1].

In Figure 1, a rectangular patch antenna is depicted. The resonance frequency of the antenna is defined by the metal patch dimensions, but also by the substrate thickness and dielectric constant. The behavior of a microstrip antenna, or commonly known also as patch antenna, can be described by different analysis methods, as the transmission-line model, the cavity model and full wave model.

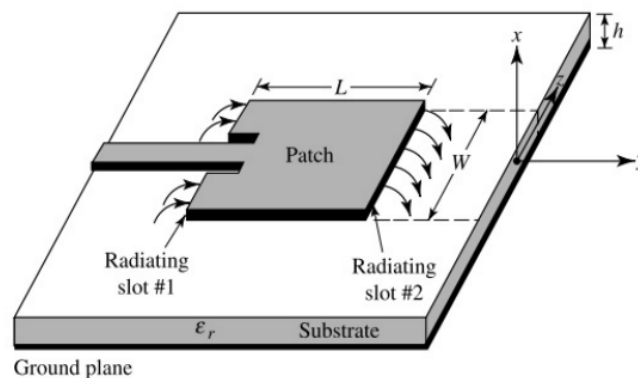
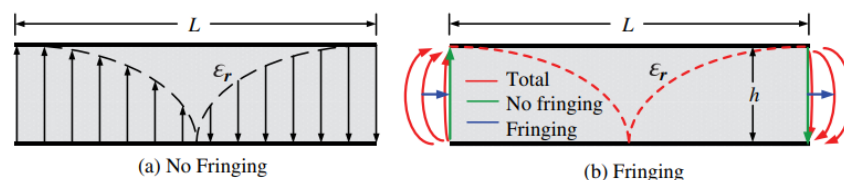


Figure 1: Illustration of a patch antenna [1]

Following the cavity model analysis, the fringing fields (Figure 2) formed on the edges of the length of the patch are the reason for the radiation.



The resonant frequency of the first order dominant mode ( $TM_{010}$ ) is defined as in equation 1, where  $f_{r010}$  is the resonant frequency,  $c_0$  is the light velocity,  $L$  is the patch length and  $\epsilon_r$  is the

dielectric constant of the substrate. More detailed description on how to design a patch antenna can be found on [1].

$$f_{r010} = \frac{c_0}{2L\sqrt{\epsilon_r}} \quad (1)$$

In order to feed the antenna, different configurations can be used, as microstrip line, aperture coupling, proximity coupling etc. The graphene patch antenna designed and presented in this report is fed by a coplanar wave guide (CPW), that consists of a thin metallic line (signal pad) on top of a dielectric with one ground electrode (ground pad) on each side of the signal pad and far away from this by a small distance (Figure 3). This kind of feed technique was chosen due to lower losses compared to a microstrip or stripline feed, providing shielding from the rest of the RF circuit resulting in a stronger signal at the receiver end.

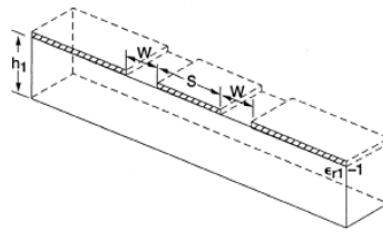


Figure 3: Representation of a CPW [2]

The impedance,  $Z_0$ , of this CPW is designed to be  $50\Omega$ .

The antenna can be described by its gain, that is defined as “the radiation power intensity in a certain direction over the total power that would be radiated by an isotropic antenna receiving the same amount of power” [1], as in equation 2, where  $G$  is the antenna gain,  $U$  is the power intensity in a certain direction and  $P_{rad}$  is the total radiated power.

$$G = \eta \frac{4\pi U}{P_{rad}} \quad (2)$$

Not only graphene-based antenna is described in this deliverable, but also other circuits based on graphene-diodes, such as power detectors (PD), analogue phase-shifter (APS) and non-linear transmission lines (NLTL), widely used in RF devices. While the NLTL are used to connect transmitters and receivers with the antennas, phase shifters are of great relevance to communications, since they can control and direct the beam radiation of antenna arrays. The use of graphene-based diodes into this kind of radio-frequency (RF) circuits leads not only to more efficient devices due to the unique graphene energy band distribution, but also the possibility to tune the operating frequency and the main radiation lobe of the antennas.

## 2 Graphene Components Designs, Simulations and Measurements

A patch antenna was defined as the design to be simulated for the future integration. Details about the antenna dimensions and simulation results are described in this chapter.

### 2.1 Graphene Patch Antenna Design

A rectangular graphene patch was chosen as the radiating element. The resonant frequency chosen for the patch antenna was 280GHz and 50 $\mu$ m polyimide substrate was used for the simulations. A metal backplane is used under the polyimide substrate. Using the already cited equations from Chapter 1, the patch antenna dimensions are the ones depicted in Table 1 below.

Antenna Parameters	Values ( $\mu$ m)
Antenna width ( $W_p$ )	355
Antenna length ( $L_p$ )	260
Substrate width ( $W_s$ )	50
Substrate length ( $L_s$ )	710
Substrate thickness ( $t_s$ )	520
Signal pad width ( $S$ )	42
Gap width between the signal and ground pads ( $g$ )	5

Table 1: Graphene patch dimensions

The transient domain solver of the simulation software CST was used to evaluate the patch antenna S11 and emitted gain. The simulation was performed with a waveguide port as excitation source for the antenna. A view of the graphene patch antenna simulated is shown in Figure 4 below. The back-metal plane, the ground-signal-ground (GSG) pad and the transmission line to the antenna were simulated using 100nm Palladium with conductivity  $1 \times 10^7$  S/m. The 50 $\mu$ m polyimide had a dielectric value of 3.5 and loss of 0.0027.

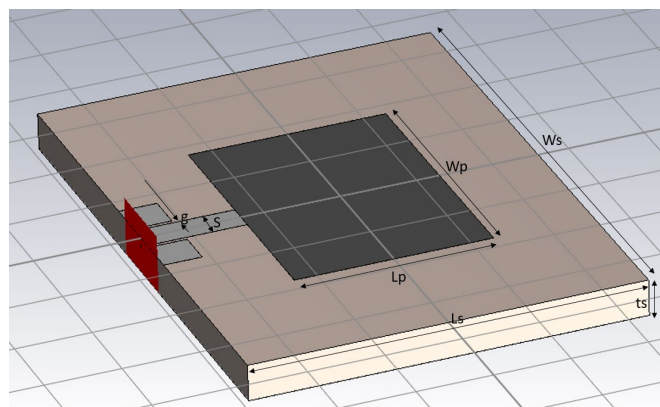


Figure 4: Graphene patch antenna simulated in CST. The antenna consists of a metal or graphene patch on top of a dielectric substrate backed by a metal plane. The antenna is driven by the GSG pads.

## 2.2 Graphene Patch Antenna Simulation Results

To compare a metal versus graphene patch antenna, a palladium patch was first simulated. Then, by adjusting values of Fermi level and relaxation time, graphene with different conductivities were simulated as the radiating patch.

In CST, graphene is modelled as a material with complex surface conductivity based on the Kubo formula, as described in equation 3.

$$\sigma = \frac{2e^2\tau}{\pi\hbar^2} K_B T \log \left( \cosh \frac{\mu_c}{2K_B T} \right) \frac{1}{1 + j\omega\tau} \quad (3)$$

Where,  $\sigma$  is the complex conductivity of graphene,  $e$  is the electric charge,  $\tau$  is the relaxation time,  $\hbar$  is the reduced Planck's constant,  $K_B$  is the Boltzmann constant,  $\mu_c$  is the chemical potential and  $\omega$  is the frequency.

The Figure 5 shows the S11 simulation result of a palladium and different graphene antennas. The metal antenna presented a resonant frequency of 282GHz and a return loss of -30dB. Regarding the graphene antennas, each conductivity value gives a different resonant frequency and return loss. In general, the resonant frequency of a graphene patch is lower compared to a metal patch of the same dimensions.

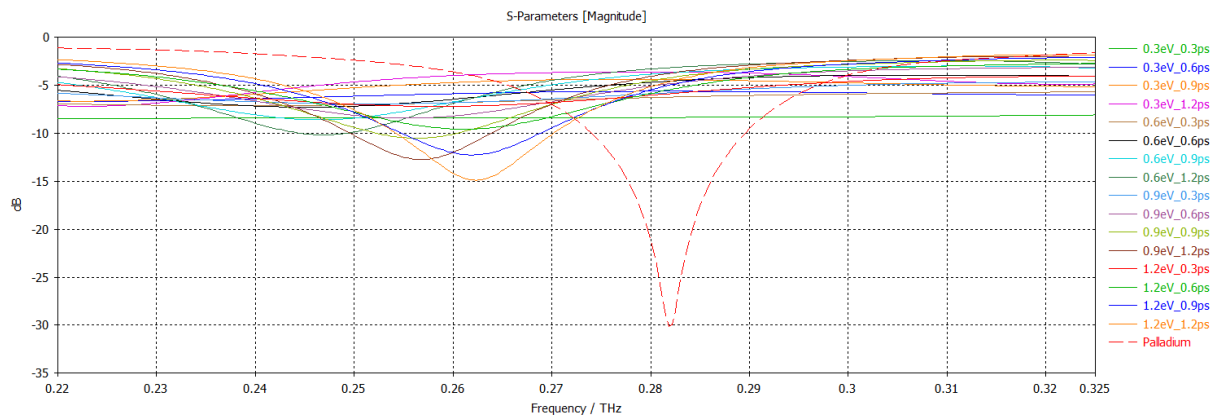


Figure 5: S11 simulated values for metal patch (dashed line) and graphene patch with different conductivity values (continuous lines)

By increasing the Fermi level of the graphene patch, it is possible to see a shift of the resonance to higher values (Figure 6). And by changing the relaxation time of the graphene, it is possible to see an improvement on the antenna behavior (Figure 7).

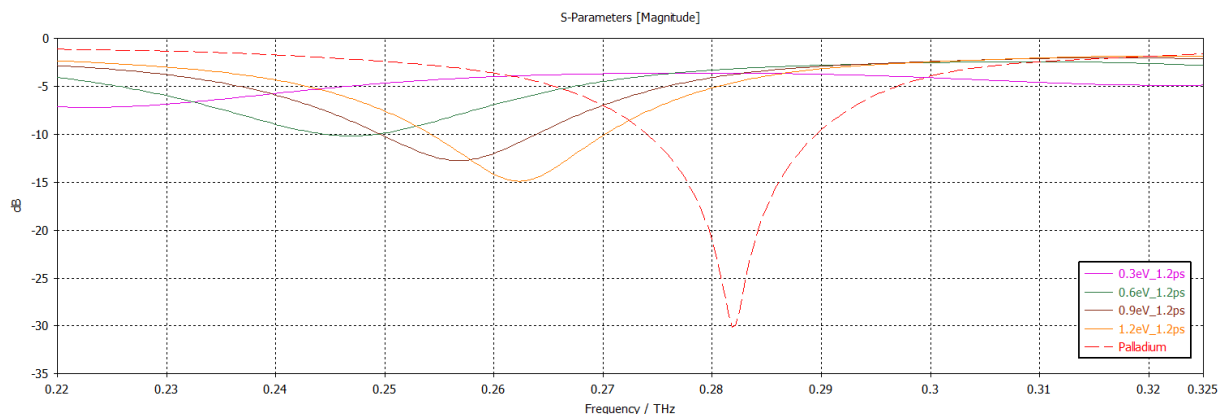


Figure 6: S11 simulation results for graphene patches with different fermi levels and relaxation time 1.2ps (continuous lines) and for a metal patch (dashed lines)

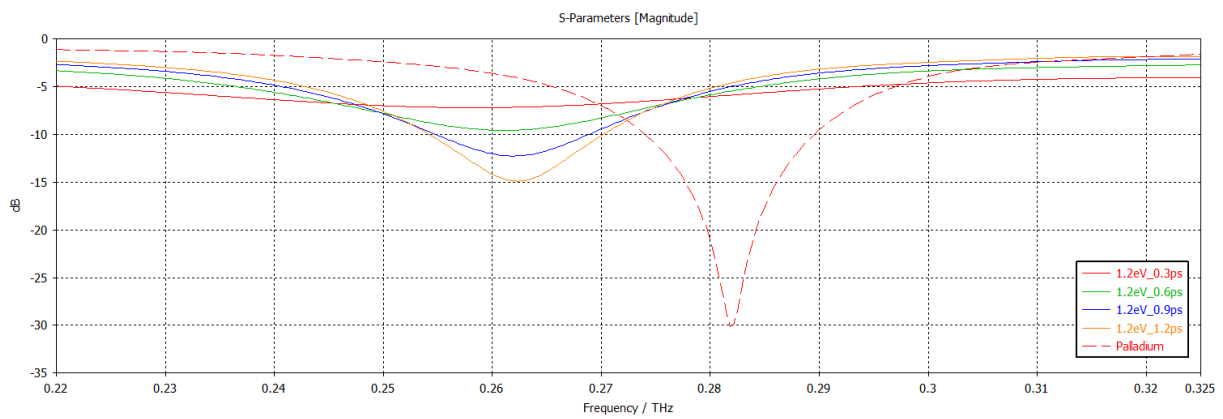


Figure 7: S11 simulation results for graphene patches with different relaxation times and Fermi level 1.2 eV (continuous lines) and metal patch (dashed line)

The emitted gain of the antennas was also simulated for the range from 220 – 325GHz (Figure 8). It is important to confirm and conclude also from here, that a high-quality graphene is needed for a proper graphene antenna patch to resonate at THz frequencies. As evident from Fig. 7 and 8, a reasonable resonance Q factor and antenna gain is only attained at a Fermi level of  $E_F = 1.2\text{eV}$  with very long scattering times above 0.9ps to 1.2 ps. It is therefore highly relevant to enhance the graphene material quality and to introduce adequate biasing contacts to be able to reach such values.

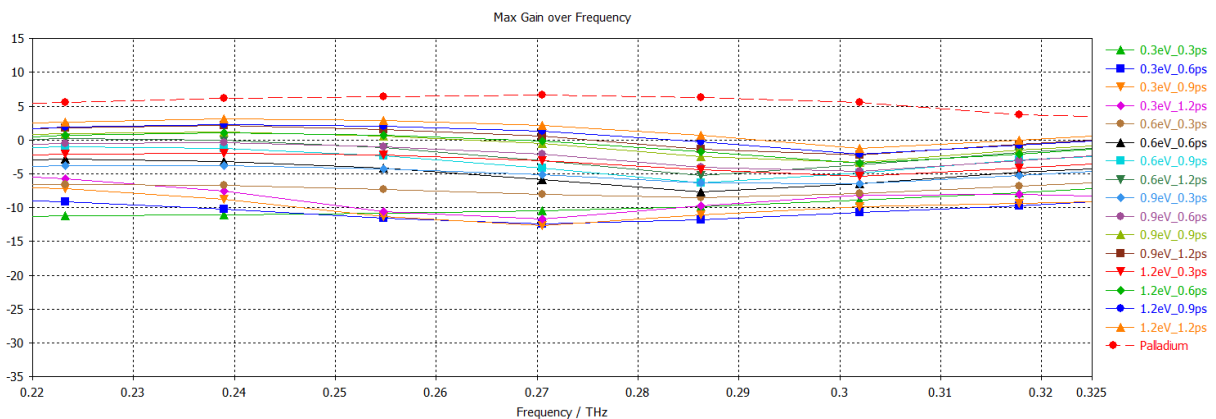


Figure 8: Maximum gain over frequency in dB of graphene patches with different conductivities (continuous lines) and metal patch (dashed line)

As an example, only the graphene patch antenna with a Fermi level of 0.9eV and relaxation time above 0.9ps and the graphene patch with Fermi level 1.2eV and relaxation time above 0.6ps presented a far field gain over 0dB. As discussed in earlier deliverables a delicate balance of Fermi level (and concomitantly charge carrier densities) and scattering rates is necessary to achieve reasonable antenna characteristics.

Using equation 4, extracted from [7], to calculate the mobility for each graphene patch simulated that could act as an antenna at THz frequencies, it is possible to translate these values in to mobilities, and to quantify the high mobilities which are required for a good THz emission of a graphene patch antenna.

$$\mu = \frac{\tau e v_f}{E_f} \quad (4)$$

The minimum mobility value required for a graphene with a Fermi level of 0.9eV to act as an antenna is 10.000cm<sup>2</sup>/Vs and for a graphene with Fermi level of 1.2eV, the minimum mobility required for the graphene is around 5.000cm<sup>2</sup>/Vs. Low values of relaxation time, can partially be compensated by higher Fermi levels. It is therefore important to explore further in the remaining part of the project how this can be achieved either by electrically biasing contacts or by chemical doping.

### 2.3 Graphene Based Circuits Design

We employed the developed graphene-diodes in circuits as power detectors (PD's), analogue phase-shifters (APS's), and nonlinear transmission lines (NLTL's)-based harmonic generators.

The in-house developed MMIC has been modified to preserve the graphene quality by doing the passivation step of graphene directly after the patterning of the graphene layer and moved the Thin-film resistor (TFR) layer to be fabricated afterwards [8], as shown in Figure 9.

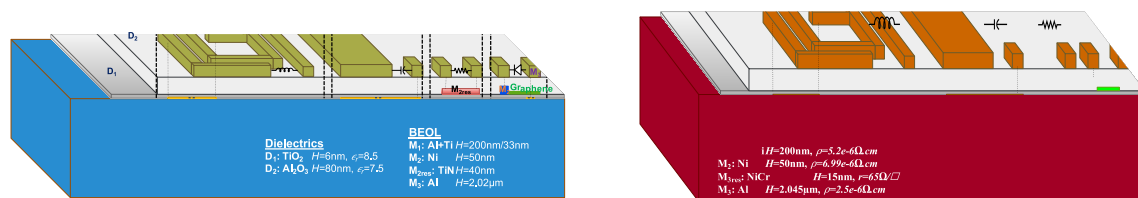


Figure 9: Old MMIC (left) versus the new MMIC (right)

The resulting pronounced graphene quality improvement is validated by Raman-shift spectroscopy after the whole fabrication, as plotted in Figure 10. From the Raman-shift spectroscopy, it is clear that there is no (or minor) D-peak, which means that there is no significant disorder in the graphene. Additionally, the 2D peak is significantly larger than the G-peak, which implies that the graphene is single-layer graphene (SLG).

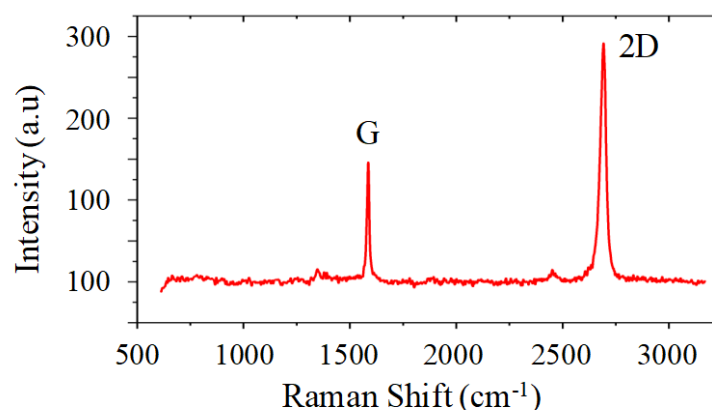


Figure 10: Raman-shift spectroscopy after fabricating the samples

This improvement in the fabrication results in a noticeable improvement in the performance and repeatability of our graphene diodes as it is shown in Figure 11, which compares the short

circuit current responsivity ( $\beta_0$ ) of the graphene diodes versus other families of diodes. Short circuit current responsivity is obtained from the I-V characteristics of the diodes and is considered as benchmark together with the Asymmetry and nonlinearity which are calculated as follows:

$$f_{Asym} = \frac{|I_F|}{|I_R|},$$

$$f_{NL} = \frac{dI/dV}{I/V},$$

$$\text{and } \beta_0 = \frac{d^2I/d^2V}{dI/dV}.$$

Such that,  $I_F$  is the forward-biased current and  $I_R$  is the reverse-biased current.

Note that figure 6 shows 2 graphene diodes; the one with the higher responsivity is the one fabricated using the new MMIC technology, while the other one was the fabricated using the old MMIC technology. Notice also that the Schottky diode is physically limited to  $20V^{-1}$  at  $300K^\circ$  due to the thermal voltage dependency.

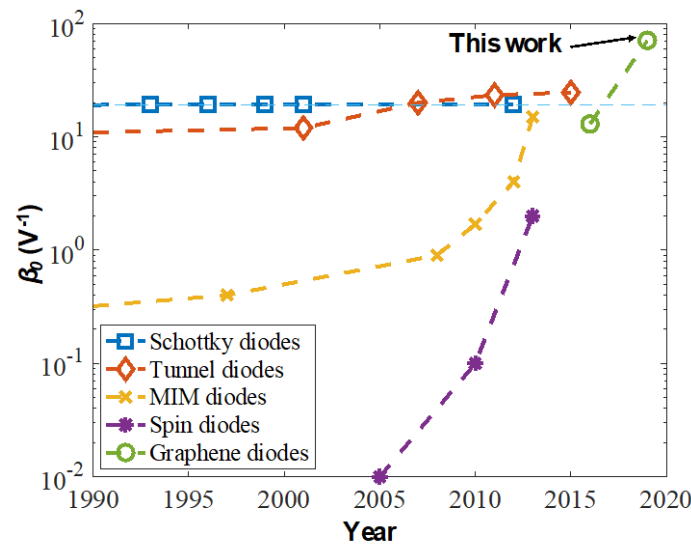


Figure 11: Short-circuit current responsivity comparison between different diode families.

### 2.3.1 Graphene diode-based APS

The designed (left) and fabricated (right) circuit of the graphene-based APS are shown in Figure 12, where three graphene-diodes are employed in a T-shaped APS architecture [9]. The chosen architecture has the advantage of compact implementation. However, the diodes D1 and D2 are in the signal path which lead to degradation in the insertion loss of the phase shifter. The circuit is designed, fabricated and measured. The fabricated prototype occupies less than  $0.42 \text{ mm}^2$  of chip area including pads. The characterization of the fabricated circuit demonstrates  $S_{11}$  better than  $-12 \text{ dB}$  for the frequency band from  $25\text{-}35 \text{ GHz}$  with a tunable phase difference of  $24^\circ$ .

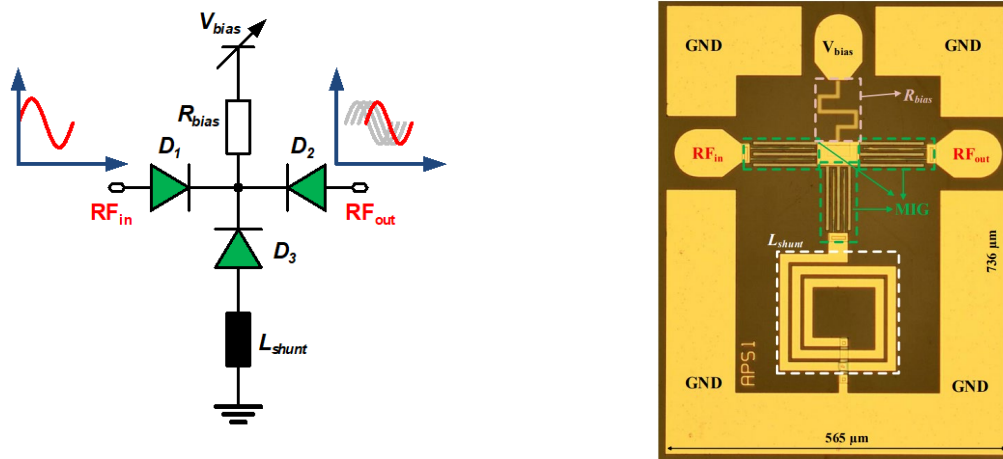


Figure 12: Graphene-based APS: schematic (left) and chip micrograph (right)

### 2.3.2 Graphene diode-based 60GHz PD with 70dB Dynamic Range

The designed (left) and fabricated (right) circuit of the graphene-based PD is shown in Figure 13, where a single graphene-diode is employed integrating the input matching and the output lowpass filter [8]. The fabricated prototype occupies 0.1 mm<sup>2</sup> of chip area including pads. Measurement results show wide input matching from 40-70 GHz with measured  $S_{11}$  better than -13 dB over the design bandwidth. The measured dynamic range is 70 dB, and the voltage responsivity is 98 V/W at 60 GHz. Measured video-bandwidth (VBW) is 2.2 GHz. The implemented input matching exploits the high frequency fringing capacitance of the top-metal while the output lowpass filter employs MIM capacitors together with the thin-film resistors (TFR).

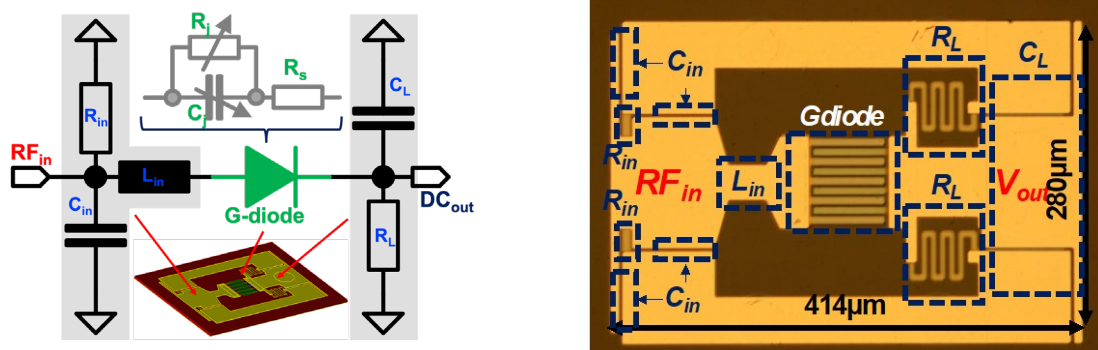


Figure 13: Graphene-based PD: schematic (left) and chip micrograph (right)

### 2.3.3 Graphene diode-based NLTL-based harmonic generator

The designed (left) and fabricated (right) circuit of the graphene-based NLTL is shown in Figure 14, where a four graphene-diodes are employed in a NLTL scheme [10]. The fabricated prototype is realized on a 500- $\mu\text{m}$  transparent quartz substrate and occupies less than 1.2 mm<sup>2</sup> of chip area including pads. Measurement results show a wide input frequency range from 0-2.8 GHz with measured  $S_{11}$  better than -10 dB. The measured second-harmonic conversion gain (CG) for an output frequency of 3.4 GHz is -21.6 dB. The measured third-harmonic CG for an output frequency of 3.15 GHz is -31 dB.

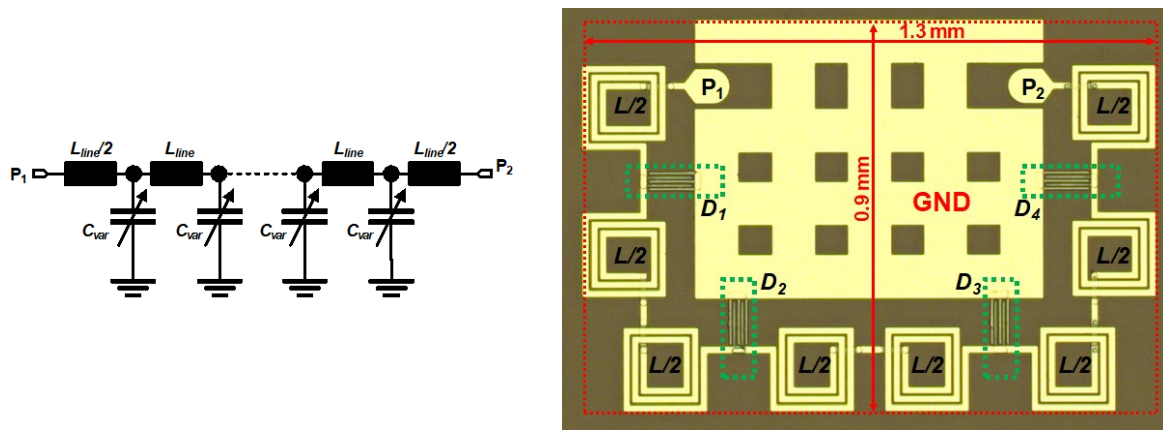


Figure 14: Graphene-based NLTL: schematic (left) and chip micrograph (right)

## 2.4 Graphene Based Circuits Measurement Results

The graphene diode-based circuits were fabricated by AMO and the validation of the fabricated prototypes was carried-out by RWTH

### 2.4.1 Graphene diode-based APS

As plotted in Figure 15, the measured  $S_{11}$  magnitude in decibels shows excellent matching for the designed frequency range at 30GHz with  $S_{11}$  better than -10dB across the whole tuning range. The measured phase of  $S_{21}$  is also plotted (right) showing a phase tuning range of up to 24 degrees at 30GHz. Further improvement in the tuning range is possible using different topologies as the reflective type APS or NLTL topology.

Graphene-based analog phase-shifters are promising candidates for beam-steering applications for smart surfaces. Accordingly, we designed in addition to the graphene-based APS circuits additional standalone metal antennae which is under measurements to combine them later.

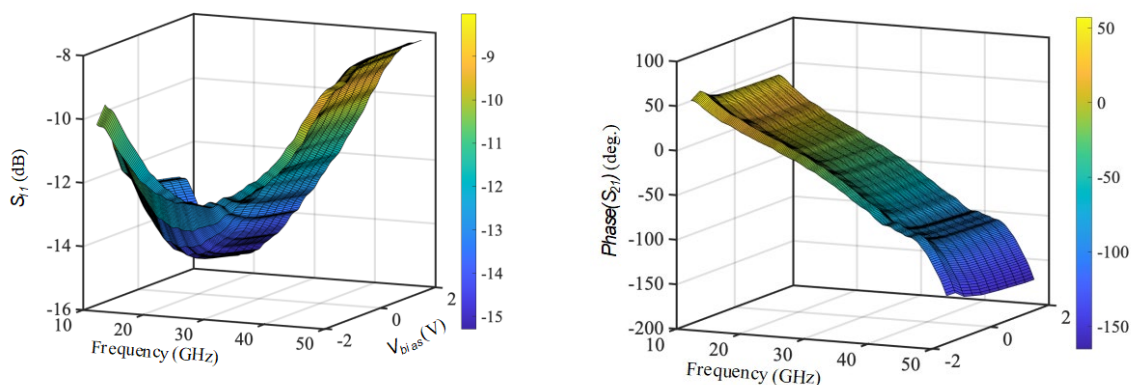


Figure 15: Measurements of the Graphene-based APS:  $\text{dB}(S_{11})$  (left) and  $\text{phase}(S_{21})$  (right).

(generally the graphene device section, very compelling scientifically, is a bit frugal in description. It would improve if we add more details and critical discussion on the characterizations and measurements)

### 2.4.2 Graphene diode-based 60GHz PD with 70dB Dynamic Range

Measurement results of the fabricated PD are plotted in Figure 16. The measured  $S_{11}$  magnitude in decibels (left) shows excellent matching for the designed frequency range at 60GHz with  $S_{11}$  better than -10dB across the whole V-band. The measured voltage sensitivity for different RF frequencies inputs (right) shows wide dynamic range of at least 70dB.

The standalone diodes are fully characterized to extract the small- and large-signal models of the diode to be used in designing the power detector circuit. The implemented design employs our MMIC high quality passives as MIM and TFR as mentioned before.

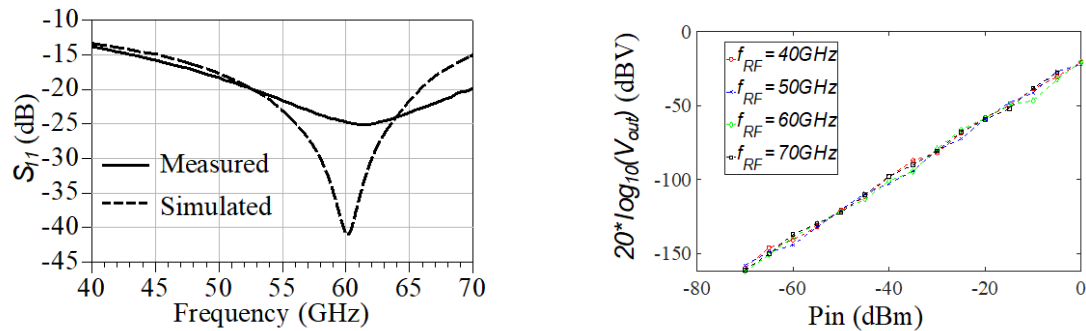


Figure 16: Measurements of the Graphene-based PD: input matching (left) and voltage sensitivity (right)

### 2.4.3 Graphene diode-based NLTL-based harmonic generator

The measured conversion gain of the 2<sup>nd</sup> (left) and 3<sup>rd</sup> (right) harmonics are plotted in Figure 17. The voltage dependency of the conversion gain validates the concept of the employment of the NLTL in frequency generation.

The measured design has promising performance to be used as a voltage tunable harmonic generator and the CVD process allows the employment of four identical graphene diodes. Additionally, the design is scalable in frequency exploiting different sizes of the graphene diodes and inductors implemented using the top-thick metal.

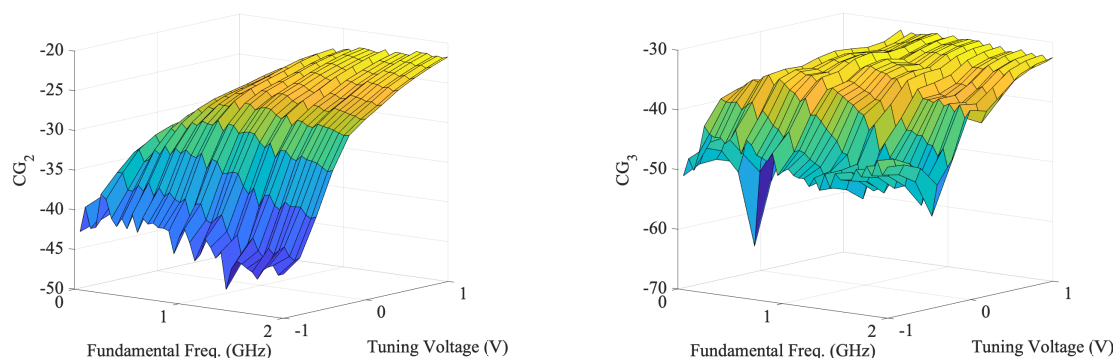


Figure 17: Measured conversion gain results of the Graphene-based NLTL: second harmonic (left) third harmonic (right)

### 3 Graphene Components Integration

The integration of the patch antenna with different dies could be implemented as shown in Figure 18. The graphene patch antenna as well as the ground-signal-ground pad will be fabricated on the front side of the polyimide substrate and the global ground patch will be on the back side of the substrate, which is in the meantime electrically connected to the ground pad on the front side. Afterwards, the Silicon-Germanium (SiGe) die or graphene based MMIC die will be bonded from the top side of the polyimide substrate. This kind of integration has been implemented in literature [7] and we have adjusted it in order to make it compatible with the technology at AMO.

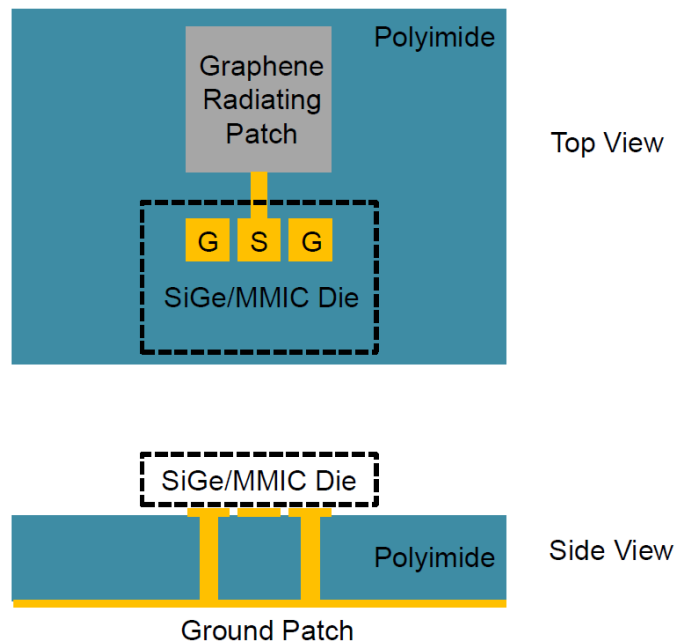


Figure 18: Integration strategy with graphene patch antenna on polyimide

The patch antenna devices are going to be manufactured in 8 $\mu$ m thick polyimide and the simulations performed by UoS will be adapted to this thickness in order to compare simulations versus measurements.

## 4 Summary of Results

The University of Siegen (UoS) was able to design and simulate a graphene-based patch antenna with resonant frequency at the THz range. Through the simulation results, the advantage with respect to a metal antenna were explored.

With the same dimensions of a metal patch antenna, a graphene antenna presents a lower resonant frequency which can be up to a factor of 100 smaller area. This could lead to a reduced chip area, since the required dimensions of a graphene patch for the same resonant frequency of a metal patch are smaller. However, at the given achievable graphene material data characteristics, antenna characteristics have a very limited performance. Present research and development concentrates on demonstrating the functionality of graphene based antennas mainly and on the achievable size reduction at a later stage. Beside of this general trend, the simulation results show the possibility for tuning the resonant frequency of the antenna by using graphene with different Fermi levels, which is a very attractive new functionality in comparison to existing antenna systems as this is not possible to accomplish with a standard metal antenna.

The schematic route to integrate the graphene-based antenna with the SiGe TRx or graphene-based MMIC components presented in this report was also shown.

The improvement in the in-house developed MMIC technology using graphene is validated by Raman spectroscopy and by measurements of the fabricated diodes. The new diodes were employed in microwave/mm-Wave circuit applications as analog phase shifters for smart surfaces, V-band power detector with an outstanding dynamic range of 70dB which is considered as a promising candidate to be employed in sixport receivers. Additionally, a NLTL is implemented employing four graphene-diodes. The developed diodes are demonstrating high potential for graphene-based circuits in high frequency applications with decent performance.

## Bibliography

- [1] B. Yao, Y. Liu and S. Huang, "Broadband gate-tunable terahertz plasmons in graphene heterostructures," *Nature Photonics*, pp. 22-28, 11 December 2017.
- [2] A. Cabellos-Aparicio, I. Llatser and A. Alarcón, "Use of Terahertz Photoconductive Sources to Characterize Tunable Graphene RF Plasmonic Antennas," *IEEE Transactions on Nanotechnology*, vol. 14, no. 2, pp. 390-396, 2015.
- [3] I. Llatser, C. Kremers and A. Ceballos-Aparicio, "Graphene-based nano-patch antenna for terahertz radiation," *Photonics and Nanostructures - Fundamentals and Applications*, vol. 10, no. 4, pp. 353-358, 2012.
- [4] M. Tamagnone, J. Gómez-Díaz and J. R. Mosig, "Reconfigurable terahertz plasmonic antenna concept using a graphene stack," *Applied Physics Letters*, vol. 101, no. 21, 21 November 2012.
- [5] C. Balanis, *Antenna Theory: Analysis and Design*, New Jersey: Wiley, 2016.
- [6] R. N. Simons, *Coplanar Waveguide Circuits, Components, and Systems*, Wiley, 2011.
- [7] X. Luo, T. Qiu, W. Lu and Z. Ni, "Plasmons in graphene: Recent progress and applications," *Materials Science and Engineering: R: Reports*, vol. 74, no. 11, pp. 351-376, 2013.
- [7] X. Luo, T. Qiu, W. Lu and Z. Ni, "Plasmons in graphene: Recent progress and applications," *Materials Science and Engineering: R: Reports*, vol. 74, no. 11, pp. 351-376, 2013.
- [8] M. Saeed et al., "Compact V-Band MMIC Square-law Power Detector with 70 dB Dynamic Range exploiting State-of-the-art Graphene diodes," 2021 IEEE MTT-S International Microwave Symposium (IMS), 2021, pp. 888-891, doi: 10.1109/IMS19712.2021.9574843.
- [9] M. Saeed, A. Hamed, E. Baskent, B. Uzlu, Z. Wang and R. Negra, "Low-cost Compact Analogue Phase-Shifter based on CVD Graphene-diode for Smart Surfaces Applications," 2021 IEEE MTT-S International Microwave Symposium (IMS), 2021, pp. 595-598, doi: 10.1109/IMS19712.2021.9574812.
- [10] M. Saeed et al., "Voltage-Tunable Thin Film Graphene-Diode-Based Microwave Harmonic Generator," in *IEEE Microwave and Wireless Components Letters*, vol. 31, no. 6, pp. 733-736, June 2021, doi: 10.1109/LMWC.2021.3061573.